



Electrodeposited IrO₂/Ti electrodes as durable and cost-effective anodes in high-temperature polymer-membrane-electrolyte water electrolyzers

Seunghoe Choe^{a,d}, Byung-Seok Lee^a, Min Kyung Cho^a, Hyoung-Juhn Kim^{a,b},
Dirk Henkensmeier^{a,b,c}, Sung Jong Yoo^{a,b}, Jin Young Kim^{a,b,c}, So Young Lee^a, Hyun S. Park^a,
Jong Hyun Jang^{a,b,c,*}

^a Fuel Cell Research Center, Korea Institute of Science and Technology (KIST), Seoul 02792, Republic of Korea

^b Division of Energy & Environment Technology, KIST School, Korea University of Science and Technology, Seoul 02792, Republic of Korea

^c Green School, Korea University, Anam-ro 145, Seongbuk-gu, Seoul 02841, Republic of Korea

^d Surface Technology Division, Korea Institute of Materials Science (KIMS), Changwon, Gyeongsangnam-do, 51508, Republic of Korea



ARTICLE INFO

Keywords:

Polymer-electrolyte-membrane water
electrolysis
High temperature
Membrane electrode assembly
IrO₂ catalyst
Electrodeposition
Titanium
Corrosion

ABSTRACT

In this study, IrO₂-coated Ti mesh (e-IrO₂/Ti) is proposed to be an efficient and durable oxygen electrode for high-temperature polymer-membrane-electrolyte water electrolyzers (HT-PEMWES). A thin IrO₂ film of sub-micron thickness was uniformly coated onto a porous Ti mesh substrate by anodic electrodeposition. The electrodeposited IrO₂ film plays the dual role of a catalyst layer for the oxygen evolution reaction (OER), and a corrosion-protection layer that prevents oxidation of the inner Ti. The e-IrO₂/Ti exhibited high performance (0.97 A cm^{-2} at 1.6 V) despite a low IrO₂ loading (0.4 mg cm^{-2}) in single-cell tests conducted at 120 °C, which is comparable to that of conventional electrodes with greater catalyst loadings ($0.8\text{--}5 \text{ mg cm}^{-2}$). Furthermore, corrosion polarization tests reveal that the IrO₂ coating physically blocks exposure of the Ti diffusion layer, thereby reducing Ti corrosion by 82% in 0.5 M H₂SO₄ at 25 °C. The low degradation rate ($1.5 \text{ mA cm}^{-2} \text{ h}^{-1}$ ($0.11\% \text{ h}^{-1}$)) obtained in aging experiments at 120 °C and 1.72 V (voltage efficiency of 85%) confirms the excellent stability of this electrode.

1. Introduction

Hydrogen is expected to be a source of future energy because it offers a clean, sustainable, and zero-carbon energy ecosystem, the “hydrogen ecosystem”, that overcomes issues related to the environment and the exhaustion of coal. Currently, however, the majority of hydrogen is produced by petrochemical processes such as the steam-reforming of natural gas (48%), partial oxidation (30%), and gasification (18%) that inevitably emit carbon into the atmosphere [1]. Water electrolysis, a technology that decomposes water into gaseous hydrogen and oxygen using electricity, provides an alternative route for the production of clean hydrogen, and has a zero- or low-carbon footprint. Currently, alkaline water electrolysis (AWE) has occupied the majority of the electrolyzer market because of its technical maturity, but relatively low hydrogen purity, the need for large-scale plants, and the use of toxic solvents have been highlighted as drawbacks [2]. As an alternative, proton exchange membrane water electrolysis (PEMWE) has received attention, especially for small-scale hydrogen production (< 300 kW) and surplus power storage in connection with renewable

power sources, due to advantages that include the high rate of hydrogen production, high hydrogen purity, small system volumes, and the absence of harmful materials [1]. In addition, the further development of PEMWE technology could be guided by its mature counterpart, the polymer electrolyte fuel cell (PEMFC).

A key limitation for the wide use of PEMWE is the relatively high price of the hydrogen produced ($4.1\text{--}8.6 \text{ € kgH}_2^{-1}$) compared to AWE ($3.2\text{--}5.0 \text{ € kgH}_2^{-1}$) [1]. The high price of PEMWE is mainly ascribed to capital costs ($0.85\text{--}2.9 \text{ € kgH}_2^{-1}$) and stack-replacement costs ($0.86\text{--}2.8 \text{ € kgH}_2^{-1}$). These devices typically operate at 60–90 °C under atmospheric pressure, which results in cell voltages of 1.55–1.8 V at 1 A cm^{-2} [3–6]. In order to reduce the cost of hydrogen production associated with PEMWE, various strategies have been suggested based on the following criteria: i) lowering the voltage loss to reduce electricity costs; ii) improving cell durability to reduce stack-replacement costs; and iii) decreasing the use of expensive materials (e.g., platinum group metals) to reduce capital and stack-replacement costs [1]. Voltage loss has been lowered by boosting the oxygen evolution reaction (OER) at the anode, which is a major contributor to voltage loss, and by

* Corresponding author at: Fuel Cell Research Center, Korea Institute of Science and Technology (KIST), Seoul 02792, Republic of Korea.
E-mail address: jhjang@kist.re.kr (J.H. Jang).

developing efficient catalysts [7–12] and membrane electrolytes [13,14]. In the meantime, cell-durability issues have been researched by using coated (Au, Pt) bipolar plates (BP) [15–17] or novel membranes [14].

High temperature PEMWEs (HT-PEMWEs) that operate at elevated temperatures (100–150 °C) are expected to provide better cell efficiencies and result in lower electricity costs [13,18–29] compared to conventional PEMWEs (60–90 °C) [3–5,10,15,30–32]. The better cell efficiency is associated with fast electrode reactions due to better electrode kinetics and lower equilibrium voltages. When the temperature is raised from 80 to 120 °C the rate constant increases by more than a factor of four because the activation energy for water splitting over the IrO₂ catalyst is 40–58 kJ mol⁻¹ [18,10]. In addition, the Nernst voltage for water splitting also decreases by 33 mV [23]. However, membrane dehydration leading to a drop in proton conductivity is severe at temperatures above the boiling point of water; hence either composite membranes such as Nafion-SiO₂ [18], Nafion-TiO₂ [19], phosphoric-acid-doped Nafion [20,24], phosphoric-acid-doped polybenzimidazole [20], and short-chain Aquion [13], or pressurized operation (2–8 bar) have been suggested as ways of overcoming this problem.

Another drawback of high-temperature operation is inferior cell stability, which inevitably increases the stack replacement cost. Ti, which is commonly utilized in diffusion-layer (DL) and BP materials, is rapidly passivated and corroded under typical HT-PEMWE operating conditions of high temperature (> 100 °C) and anodic potential (> 1.0 V_{SHE}) [33,34]. For example, Malis et al. reported that during water electrolysis using a Ti-based DL and BP, the current density at 1.7 V gradually decreased, at a rate of 0.21% h⁻¹ (110 °C) and 0.23% h⁻¹ (150 °C) along with increases in ohmic resistance [29]. Hence, a further study is required in order to clarify the stability of Ti during HT-PEMWE operation, and to develop a method that ensures the stability of Ti DLs and Ti BPs.

In this study, electrodeposited IrO₂ is proposed to be a corrosion-protective film that suppresses the passivation of the inner Ti substrate, while also acting as a cost-effective catalyst layer for OER. The excellent catalytic activity of anodically electrodeposited IrO₂ toward OER, even at very low catalyst loading, has been previously revealed by us [33,34]. In this study, we investigated whether or not the electrodeposited IrO₂ catalyst could protect the Ti DL from corrosion during HT-PEMWE operation. An IrO₂ film of submicron thickness was uniformly deposited over the entire surface of porous Ti mesh via anodic electrodeposition. The properties of the IrO₂ film were examined and the performance and stability of this electrode were assessed at the single-cell level.

2. Experimental

2.1. Preparation and characterization of the oxygen electrode

The oxygen electrode (anode) was prepared by either electrodeposition or spraying methods on two kinds of diffusion layers (Ti and carbon paper (CP)). A solution consisting of 10 mM iridium chloride hydrate (IrCl₄·H₂O), 100 mM hydrogen peroxide (H₂O₂), 40 mM oxalic acid (COOH₂·2H₂O), and 340 mM potassium carbonate (K₂CO₃) was prepared as the electrodeposition solution [33,34]. The IrO₂/Ti (e-IrO₂/Ti) electrode was prepared via electrodeposition on the Ti mesh substrate (Ti gauze 80 mesh, Alpha Aeaser) at various deposition potentials (E_{dep}, 0.5–0.8 V_{SCE}) and deposition times (t_{dep}, 1–20 min) at room temperature. Ti mesh with an active area of 32 cm² and the standard calomel electrode (SCE) were employed as counter and reference electrodes, respectively. For comparison, the e-IrO₂/CP electrode was also prepared by electrodepositing IrO₂ (E_{dep} = 0.7 V and t_{dep} = 10 min) on carbon paper (TGPH-090, Toray). All processes were carried out with a potentiostat (AUT302N, AUTO LAB Ltd.). In addition, the sprayed IrO₂/Ti (s-IrO₂/Ti) electrode was prepared by spraying the

catalyst ink (IrO₂·2H₂O (Alfa Aesar), 5 wt% Nafion solution (DuPont Co.), deionized water, and isopropyl alcohol) onto the substrate. The amount of loaded IrO₂ was controlled to be 1.0 mg cm⁻².

The surface morphology and IrO₂ distribution on the substrate were examined with field emission scanning electron microscopy (FE-SEM, Inspect F50, Field Emission Inc.) and electron-probe micro analysis (EPMA, JXA-8500F, JEOL). The cross-sectional views of the prepared samples were analyzed using a focused ion beam (FIB, Nova 600, FEI) after the deposition of a Pt protecting layer. X-ray photoelectron spectroscopy (XPS, PHI 5000 VersaProbe, Ulvac-PHI Ltd.) using Al K α (1486.6 eV) radiation, and inductively coupled plasma mass spectroscopy (ICP-MS, iCAP 6300 series, Thermo Ltd.) were employed to check the oxidation state of Ir and the amount of loaded IrO₂, respectively. The corrosion behavior of the DL was examined using linear sweep voltammetry at a scan rate of 1 mV s⁻¹ over the -0.8–1.0 V_{SCE} potential range in 0.5 M H₂SO₄ solution at 25 °C. Ti mesh and SCE were used as the counter and reference electrodes, respectively.

2.2. HT-PEMWE single-cell experiments

The single cell was fabricated by assembling the following components: cathode end plate, graphite BP, hydrogen electrode, Nafion membrane (NR-212, DuPont), oxygen electrode, Au/Ti BP, and anode end plate. Both oxygen and hydrogen electrodes had active areas of 6.25 cm². The hydrogen electrode was prepared by spraying the catalyst ink (46.5 wt% Pt/C (TKK), 5 wt% Nafion solution, deionized water and isopropyl alcohol) onto commercial carbon paper (39BC, SGL carbon). The Pt loading was controlled to be 0.4 mg cm⁻².

With deionized water (15 mL min⁻¹) flowing into the anode, iV curves and electrochemical impedance spectroscopy (EIS) spectra were obtained using a potentiostat (HCP-803, biologic) at 120 °C and 2.5 bar. iV curves were obtained by applying sequential constant voltages over the 1.35–2.0 V range, at intervals of 0.05 V, and the mean current density was obtained over 60 s. EIS measurements were conducted at DC potentials of 1.72 V and an AC frequency that ranged from 50 kHz to 50 mHz. Degradation experiments were carried out at a constant voltage of 1.72 V (voltage efficiency: 85%) at 120 °C and 2.5 bar.

3. Results and discussion

3.1. Fabrication and characterization of e-IrO₂/Ti electrodes

Anodic electrodeposition of IrO₂ on Ti mesh was conducted with E_{dep} values of 0.5–0.9 V_{SCE}; the current profiles during IrO₂ electrodeposition is presented in Fig. 1. As shown, the current density was low at 0.5 V_{SCE} and 0.6 V_{SCE}. However, when E_{dep} was increased to 0.7–0.9 V_{SCE}, the current gradually increased due to higher levels of [Ir]

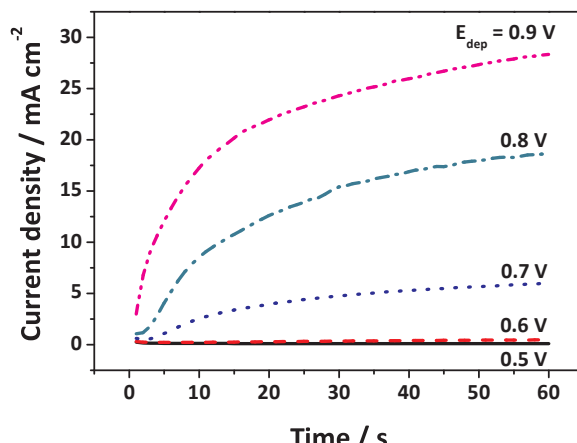


Fig. 1. Current profiles during IrO₂ electrodeposition at E_{dep} values of 0.5–0.9 V_{SCE}.

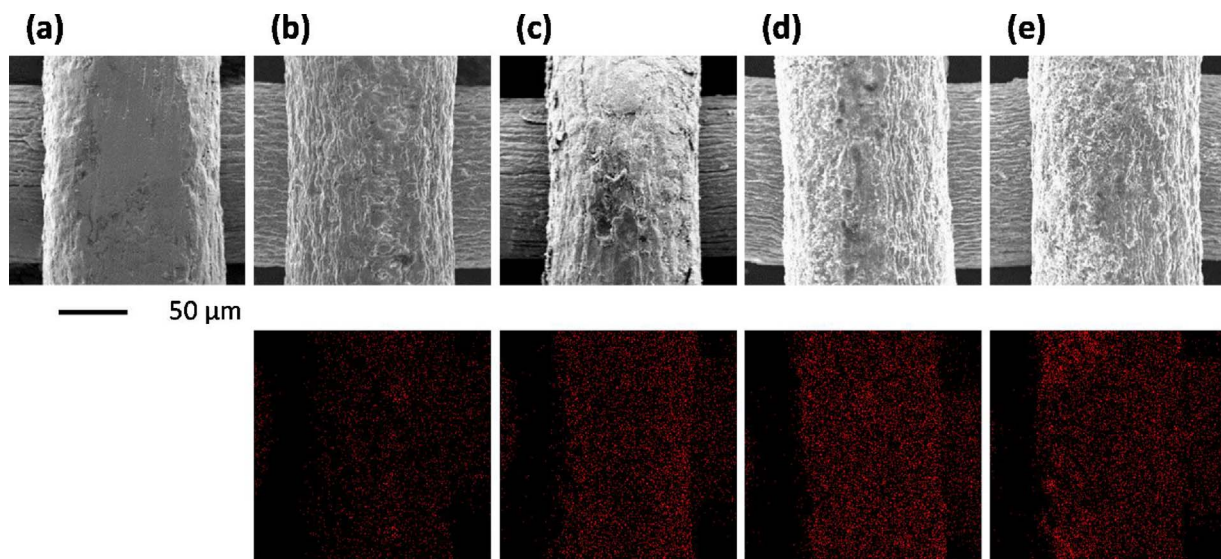


Fig. 2. Surface morphologies of (a) pristine Ti mesh and (b)–(e) the IrO_2 -deposited Ti mesh ($\text{e-}\text{IrO}_2/\text{Ti}$) at (b) 0.6, (c) 0.7, (d) 0.8, and (e) 0.9 V_{SCE} over 5 min. The corresponding Ir EPMA maps are also shown.

$(\text{COO})_2(\text{OH})_4^{2-}$ -complex oxidation (to IrO_2) at the anode together with OER catalyzed by IrO_2 [34]. At 0.7–0.9 V_{SCE} , the current rapidly increased over the initial 10 s, after which growth slowed down; this observation can be explained by higher OER activity on the deposited $\text{e-}\text{IrO}_2$ compared to the bare Ti substrate.

Surface morphologies and corresponding EPMA maps of the electrodes with various E_{dep} s are presented in Fig. 2. Even at an E_{dep} value of 0.6 V_{SCE} , where the current density was low (Fig. 1), a small amount of IrO_2 was observed on the Ti surface (Fig. 2b). With increasing E_{dep} (to 0.7 V_{SCE}), the amount of deposition increased, and the Ti surface became fully covered by the IrO_2 film without any noticeable cracks (Fig. 2c). At 0.8 V_{SCE} and 0.9 V_{SCE} , IrO_2 was still uniformly deposited on the Ti surface, and electrode detachment that had previously been observed on the $\text{e-}\text{IrO}_2/\text{CP}$ electrode at the same E_{dep} values [34] was not observed. The absence of IrO_2 detachment at high E_{dep} indicates good adhesion between IrO_2 and the Ti surface. Except at 0.6 V_{SCE} , where IrO_2 was rarely seen, the IrO_2 surface coverage did not significantly vary between 0.7 and 0.9 V_{SCE} . Further experiments were carried out at an E_{dep} of 0.7 V_{SCE} , where full coverage is expected with high efficiency.

The oxidation state of the electrodeposited Ir film on Ti ($E_{\text{dep}} = 0.7 \text{ V}_{\text{SCE}}$, $t_{\text{dep}} = 5 \text{ min}$) was confirmed by XPS. As shown in Fig. 3, two asymmetric Ir 4f peaks were observed at 65.1 (4f_{5/2}) and 62.2 eV (4f_{7/2}); each peak was fitted by two Gaussian curves. The peaks with lower binding energies, at 65.10 eV (4f_{5/2}) and 62.10 eV (4f_{7/2}),

are assigned to the Ir^{4+} state [35–37], while the higher binding energy peaks, at 66.55 eV (4f_{5/2}) and 63.55 eV (4f_{7/2}), correspond to the unscreened components of an Ir^{4+} state [11,38]. Hence, the deposited surface was mainly composed of IrO_2 .

The time evolution of the IrO_2 film at a fixed E_{dep} of 0.7 V_{SCE} is presented in Fig. 4. At the short t_{dep} of 1 min (Fig. 4a), the film phase that formed on the Ti is indicative of high IrO_2 nucleation density followed by rapid film formation. Until a t_{dep} of 5 min (Fig. 4b and c), the IrO_2 film grew uniformly on the Ti surface without the formation of any surface defects. However, when t_{dep} was increased to 10 and 20 min (Figs. 4d and e), cracks and IrO_2 agglomerates began to form; similar crack formation at high t_{dep} was observed for the $\text{e-}\text{IrO}_2/\text{CP}$ electrode in our former report [34].

Fig. 5a shows that the IrO_2 loading at an E_{dep} of 0.7 V_{SCE} gradually increased with deposition time (t_{dep}): 0.01 mg cm^{-2} (1 min) $\rightarrow 0.40 \text{ mg cm}^{-2}$ (5 min) $\rightarrow 2.69 \text{ mg cm}^{-2}$ (20 min). From the slope ($0.141 \text{ mg cm}^{-2} \text{ min}^{-1}$), the apparent current efficiency was determined to be $\sim 15\%$, indicating that part of the electric charge was consumed by the OER during IrO_2 deposition. Fig. 5b displays a cross-sectional image of the $\text{e-}\text{IrO}_2/\text{Ti}$ electrode ($E_{\text{dep}} = 0.7 \text{ V}_{\text{SCE}}$, $t_{\text{dep}} = 5 \text{ min}$) analyzed by FIB-SEM after being coated with a protective Pt layer. This figure clearly shows that the IrO_2 layer uniformly covers the entire surface of the Ti substrate, which is desirable for the prevention of the oxidation of the Ti surface and for the enhancement of PEMWE durability. From the average thickness (183 nm), the apparent density of the amorphous $\text{e-}\text{IrO}_2$ film [39–41] was determined to be 8.63 g cm^{-3} , which is lower than that of bulk crystalline IrO_2 (11.66 g cm^{-3}) [34,42]. As this $\text{e-}\text{IrO}_2$ film has a much higher density than a previously reported amorphous film (2 g cm^{-3}) fabricated by constant current deposition at $35 \mu\text{A cm}^{-2}$ [41], the $\text{e-}\text{IrO}_2$ in this study is expected to have very small amounts of internal pores and therefore superior protection against corrosion.

3.2. HT-PEMWE single cell performances

The performance of the $\text{e-}\text{IrO}_2/\text{Ti}$ electrode ($E_{\text{dep}} = 0.7 \text{ V}_{\text{SCE}}$, $t_{\text{dep}} = 1\text{--}20 \text{ min}$) was evaluated by single-cell experiments at 120°C and 2.5 bar (Fig. 6a). When t_{dep} was increased from 1 to 5 min, water-electrolysis performance gradually improved; the current density at 1.6 V gradually increased from 0.07 to 0.96 A cm^{-2} . While the IrO_2 loading increased from 0.01 to 0.40 mg cm^{-2} , no significant change in electrode morphology was observed by FE-SEM. With further increases

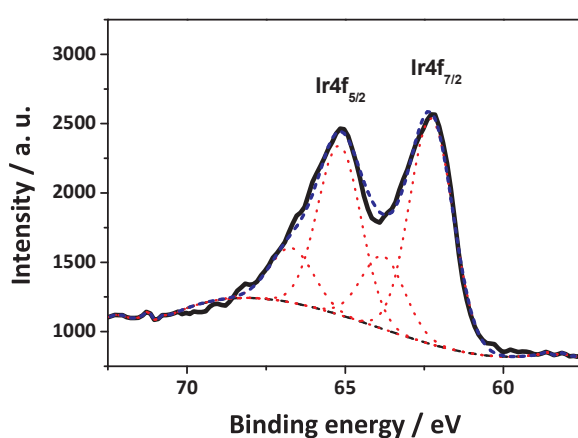


Fig. 3. The XPS spectrum of $\text{e-}\text{IrO}_2/\text{Ti}$ deposited at 0.7 V_{SCE} for 5 min.

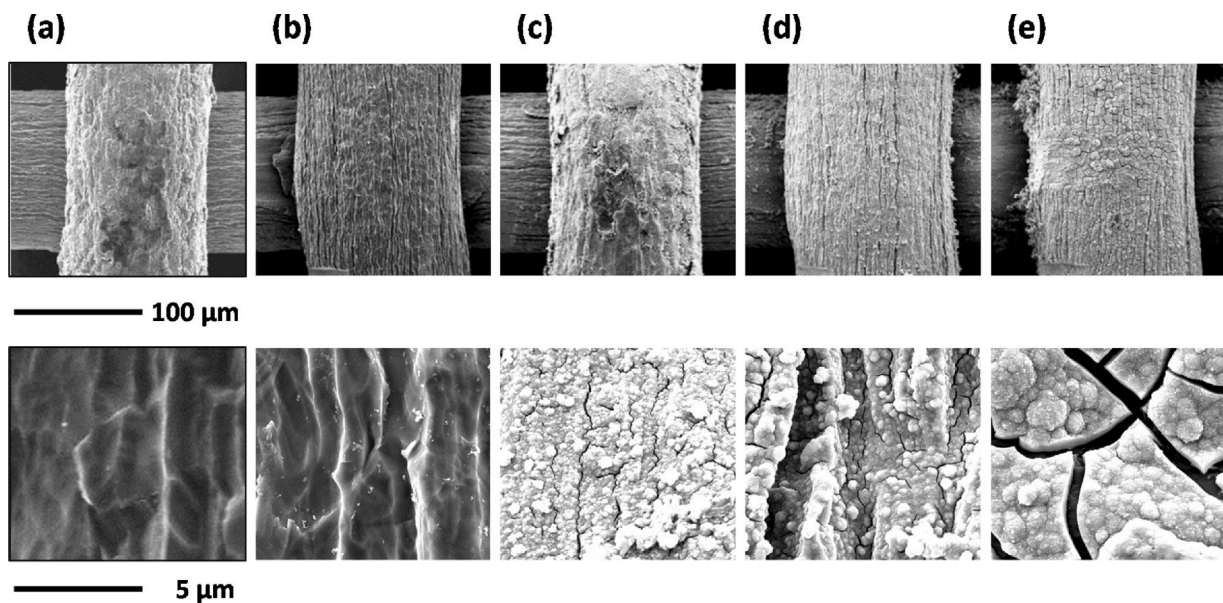


Fig. 4. Time-evolution of e-IrO₂/Ti morphology. Electrodes were prepared by controlling t_{dep} to: (a) 1, (b) 3, (c) 5, (d) 10, and (e) 20 min at a fixed E_{dep} of 0.7 V_{SCE}.

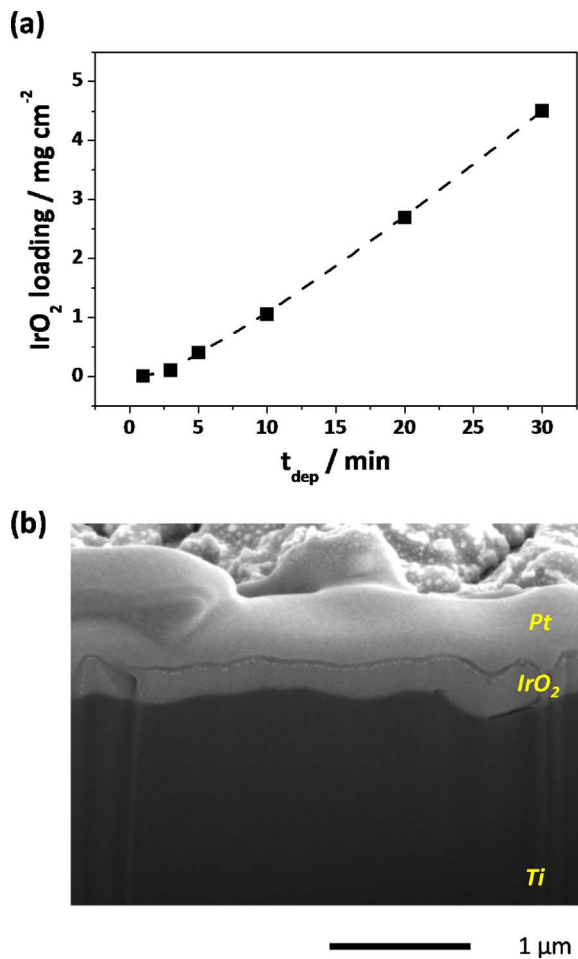


Fig. 5. (a) IrO_2 loading as function of t_{dep} at a fixed E_{dep} of 0.7 V_{SCE}. (b) The cross-sectional image of the e-IrO₂/Ti ($E_{dep} = 0.7 \text{ V}$, $t_{dep} = 5 \text{ min}$) electrode.

in t_{dep} , single-cell performance was observed to decrease, exhibiting current densities at 1.6 V of 0.67 A cm^{-2} (10 min) and 0.38 A cm^{-2} (20 min), even though the IrO_2 loading increased to 1.05 mg cm^{-2} and 2.70 mg cm^{-2} , respectively. These experimental results indicate that

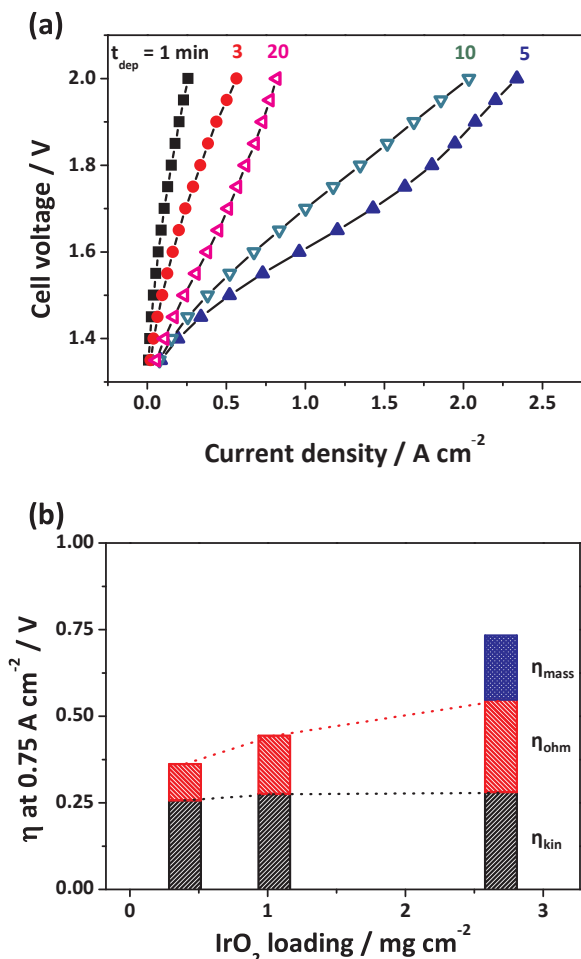


Fig. 6. (a) iV curves for e-IrO₂/Ti-electrode-deposited MEAs with varying values of t_{dep} at a fixed E_{dep} of 0.7 V_{SCE}. (b) Kinetic (η_{kin}), ohmic (η_{ohm}), and mass transfer (η_{mass}) overpotentials at 0.75 A cm^{-2} for e-IrO₂/Ti (t_{deps} of 5, 10, and 20 min).

while the IrO_2 catalyst loading is an important factor for low loadings, there are other factors that decrease electrolysis performance at high loadings.

In order to elucidate the reason for the observed decay in performance at t_{dep} values higher than 5 min, an overpotential analysis was performed according to the procedure in our previous report [33]. Fig. 6b displays the kinetic, ohmic, and mass overpotentials at a current density of 0.75 A cm^{-2} . As the IrO_2 loading increased from 0.40 mg cm^{-2} ($t_{dep} = 5 \text{ min}$) to 2.70 mg cm^{-2} (20 min), the kinetic overpotential (η_{kin}) did not change significantly, indicating that higher IrO_2 loading does not provide further active sites and therefore does not affect overall cell performance. However, the ohmic loss (η_{ohm}) gradually increased: 0.105 V ($t_{dep} = 5 \text{ min}$) $\rightarrow 0.168 \text{ V}$ (10 min) $\rightarrow 0.267 \text{ V}$ (20 min), which is possibly attributable to Ti surface oxidation at the cracks in the IrO_2 film that forms nonconductive TiO_2 layers. Initially the entire Ti surface is covered and protected by the uniform IrO_2 film, but prolonged IrO_2 electrodeposition produces cracks in the IrO_2 film, exposing part of the Ti surface to the electrolyte solution and allowing time for TiO_2 to grow under oxidative conditions. In addition, at a current density of 0.75 A cm^{-2} , the mass transfer overpotential (η_{mass}) was negligible at $t_{dep} = 5$ and 10 min, but became significant (0.185 V) at $t_{dep} = 20 \text{ min}$. We expect that an increase in hydrophobicity due to surface roughening [43,44], or O_2 trapped on the cracked IrO_2 surface, induces mass-transfer limitations.

Fig. 7a compares the HT-PEMWE current density of the e- IrO_2/Ti anode at 1.6 V (120°C) with those previously reported in the literature ($110\text{--}130^\circ\text{C}$) [13,18–20,23–28], as functions of anode-catalyst loading. The e- IrO_2 electrode in this study provided a high current density of 0.96 A cm^{-2} even though the anode catalyst loading was very low

(0.4 mg cm^{-2}). It should be noted that slightly higher current densities ($1.1\text{--}1.3 \text{ A cm}^{-2}$) were reported by three groups that studied the short-chain Aquion membrane [13], the $\text{Ru}_{0.7}\text{Ir}_{0.3}\text{O}_2$ catalyst [23], and diffusion layer optimization [27]. However, their catalyst loadings were more than 3.75 times higher than those in this study: 2 mg cm^{-2} [13], 2.5 mg cm^{-2} [23], and 1.5 mg cm^{-2} [27]. We therefore conclude that very high catalyst utilization was achieved in the present study. Fig. 7b shows the mass activities of the various catalysts, which were calculated by dividing the respective current density by the anode loading. As discussed, the mass activity of the HT-PEMWE single cell in this study was as high as 2.43 A mg^{-1} , which is about four times that of the best value in the literature (0.63 A mg^{-1}) [27]. This result clearly indicates that the e- IrO_2/Ti electrode is highly efficient and cost effective.

3.3. Stability of e- IrO_2/Ti electrodes

As mentioned in earlier, the electrodeposited IrO_2 catalyst is expected to protect the Ti DL from oxidation, as oxide formation during HT-PEMWE operation is considered to be a major degradation mechanism [45,46]. The effect of the electrodeposited IrO_2 layer on Ti stability was determined by polarization analysis in a three-electrode cell with $0.5 \text{ M H}_2\text{SO}_4$ aqueous solution. The stability of a passivation film can be evaluated by the critical current density (i_c) and the passivation current density (i_p), which correspond to the peak current and the stabilized current density during the anodic sweep from OCP, respectively. As shown in the inset of Fig. 8, pristine Ti ($t_{dep} = 0 \text{ min}$) exhibited an open circuit potential (OCP) of $-0.18 \text{ V}_{\text{SCE}}$, which is consistent with the report of Devilliers et al. for a Ti disk (99.6% purity) in $0.5 \text{ M H}_2\text{SO}_4$ [47]. On sweeping the potential in the positive direction, the i_c was determined to be $31.76 \mu\text{A cm}^{-2}$ from the peak current at $0.02 \text{ V}_{\text{SCE}}$ where the passivation begins, while i_p was determined to be $26 \sim 30 \mu\text{A cm}^{-2}$. When IrO_2 was deposited on the Ti DL, the i_c significantly decreased to 8.18 (1 min), $5.66 \mu\text{A cm}^{-2}$ (5 min), and 5.68 (10 min), clearly verifying the protective effect of the IrO_2 film. Note that the passivation current density of the IrO_2 -coated samples could not be determined due to the overlap of the $\text{Ir}^{3+}/\text{Ir}^{4+}$ redox currents at around $0.8 \text{ V}_{\text{SCE}}$ (Fig. 9).

For the e- IrO_2/Ti , s- IrO_2/Ti , and e- IrO_2/C electrodes, durability was evaluated by operating HT-PEMWE single cells at 1.72 V , which corresponds to a voltage efficiency of 85% (120°C and 2.5 bar). The current density of e- IrO_2/Ti gradually decreased from 1.30 A cm^{-2} to 0.83 A cm^{-2} over 300 h , which corresponds to a degradation rate of $1.5 \text{ mA cm}^{-2} \text{ h}^{-1}$ or $0.11\% \text{ h}^{-1}$. In contrast, the conventional spray-type electrode (s- IrO_2/Ti) exhibited severe degradation during the initial 25 h ($9.6 \text{ mA cm}^{-2} \text{ h}^{-1}$, $1.20\% \text{ h}^{-1}$) and, during further operation to

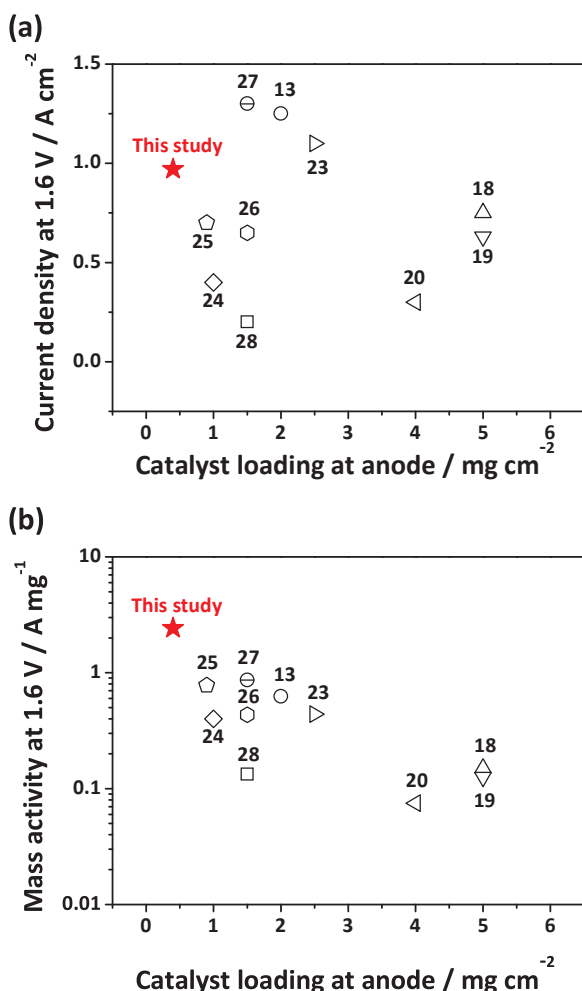


Fig. 7. (a) Current density and (b) mass activity for e- IrO_2/Ti ($E_{dep} = 0.7 \text{ V}_{\text{SCE}}$) electrodes at 1.6 V , 120°C and 2.5 bar as functions of anode catalyst loading. Data from previous reports at operating temperatures of $110\text{--}130^\circ\text{C}$ are also presented.

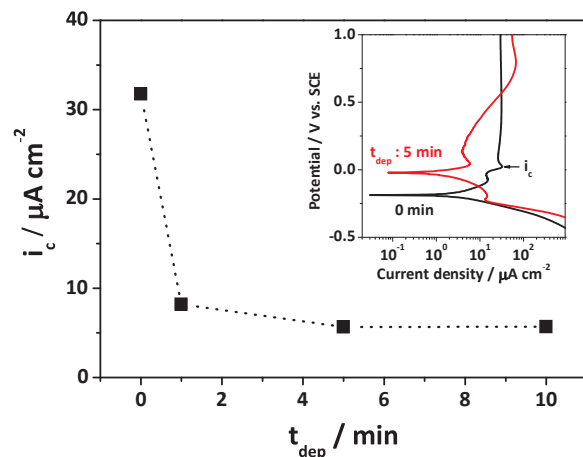


Fig. 8. Polarization curves for pristine and IrO_2 -electrodeposited ($E_{dep} = 0.7 \text{ V}_{\text{SCE}}$) Ti meshes in $0.5 \text{ M H}_2\text{SO}_4$ at 25°C . The inset shows the critical current density as a function of t_{dep} .

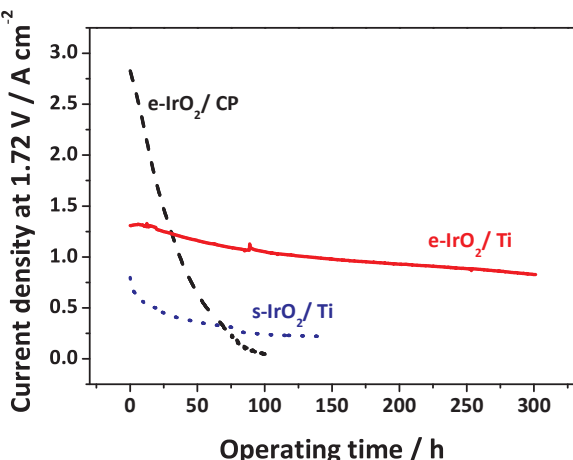


Fig. 9. Performance decays during single-cell operation at 1.72 V, 120 °C and 2.5 bar for the e-IrO₂/Ti, e-IrO₂/CP, and s-IrO₂/Ti electrodes.

150 h, the rate of degradation decreased, resulting in overall degradation rate of 3.93 mA cm⁻² h⁻¹ (0.48% h⁻¹). Therefore, we conclude that the IrO₂ layer in the e-IrO₂/Ti electrode is effectively utilized as a corrosion-resistive coating layer as well as an OER electrocatalyst, resulting in significantly enhanced HT-PEMWE durability. In the case of the e-IrO₂/CP electrode, the current density decreased rapidly, from 2.84 A cm⁻² to 0.05 A cm⁻² over 100 h (49.4 mA cm⁻² h⁻¹ (1.74% h⁻¹)), confirming that a durable material is required for the anode DL in HT-PEMWE cells. It should be noted that Malis et al. tested HT-PEMWE with a Ti felt DL at 1.7 V and reported a degradation rate of 0.21% h⁻¹ at 110 °C and 0.23% h⁻¹ at 150 °C [29], which is about twice that of the e-IrO₂/Ti in this study (0.11% h⁻¹). In the case of the study by Antonucci et al., HT-PEMWE operation with a hydrophobized Ti DL was carried out at a much lower voltage, 1.5 V, and a low degradation rate of 0.1% h⁻¹ was observed (120 °C) [18].

4. Conclusions

e-IrO₂ is proposed to be an efficient catalyst for the oxygen evolution reaction as well as a corrosion-protection film for the inner Ti diffusion layer in HT-PEMWE applications. An elaborate IrO₂ film of submicron thickness was uniformly coated on porous Ti mesh via anodic electrodeposition. The IrO₂ coating acts not only an OER catalyst but also as a protective film against Ti oxidation. This electrode exhibited a current density of 0.96 A cm⁻² at 1.6 V and 120 °C with an IrO₂ loading of 0.4 mg cm⁻², which is comparable to electrodes with higher IrO₂ loadings (0.8–5 mg cm⁻²) previously reported in the literature. The degradation rate of a cell operated at 1.72 V and 120 °C was 1.5 mA cm⁻² h⁻¹ (0.11% h⁻¹), confirming the stability of the e-IrO₂/Ti electrode for HT operation.

Acknowledgement

This work was supported by the New & Renewable Energy Core Technology Program of the Korea Institute of Energy Technology Evaluation and Planning (KETEP), a granted financial resource of the Ministry of Trade, Industry & Energy, Republic of Korea (No. 20143010031770 and No. 20153010041750). This study was also financially supported by KIST through the Institutional Project.

References

- [1] L. Bertuccioli, A. Chan, D. Hart, F. Lehner, B. Madden, E. Standen, Tech. Rep. E4tech Elec. Energy (2017), http://www.fch.europa.eu/sites/default/files/study%20electrolyser_0-Logos_0_0.pdf.
- [2] J.D. Holladay, J. Hu, D.L. King, Y. Wang, Catal. Today 139 (2009) 244–260.
- [3] C. Rozain, E. Mayousse, N. Guillet, P. Millet, Appl. Catal. B 182 (2016) 153–160.
- [4] P. Millet, R. Ngameni, S.A. Grigoriev, N. Mbemba, F. Brisset, A. Ranjbari, C. Etiévant, Int. J. Hydrol. Energy 35 (2010) 5043–5052.
- [5] S.A. Grigoriev, P. Millet, S.A. Volobuev, V.N. Fateev, Int. J. Hydrol. Energy 34 (2009) 4968–4973.
- [6] P. Millet, N. Mbemba, S.A. Grigoriev, V.N. Fateev, A. Aukaloo, C. Etiévant, Int. J. Hydrol. Energy 36 (2011) 4134–4142.
- [7] H.N. Nong, H.S. Oh, T. Reier, E. Willinger, M.G. Willinger, V. Petkov, D. Teschner, P. Strasser, Angew. Chem. 54 (2015) 2975–2979.
- [8] S. Siracusano, N. Van Dijk, E. Payne-Johnson, V. Baglio, A.S. Aricò, Appl. Catal. B 164 (2015) 488–495.
- [9] V.H. Tran, T. Yatabe, T. Matsumoto, H. Nakai, K. Suzuki, T. Enomoto, T. Hibino, K. Kaneko, S. Ogo, Chem. Commun. (Camb) 51 (2015) 12589–12592.
- [10] P. Lettenmeier, L. Wang, U. Golla-Schindler, P. Gazdzicki, N.A. Canas, M. Handl, R. Hiesgen, S.S. Hosseiniy, A.S. Gago, K.A. Friedrich, Angew. Chem. 55 (2016) 742–746.
- [11] L.C. Seitz, C.F. Dickens, K. Nishio, Y. Hikita, J. Montoya, A. Doyle, C. Kirk, A. Vojvodic, H.Y. Hwang, J.K. Norskov, T.F. Jaramillo, Science 353 (2016) 1011–1014.
- [12] L. Wang, V.A. Saveljeva, S. Zafeiratos, E.R. Savinova, P. Lettenmeier, P. Gazdzicki, A.S. Gago, K.A. Friedrich, Nano Energy 34 (2017) 385–391.
- [13] A. Skulimowska, M. Dupont, M. Zaton, S. Sunde, L. Merlo, D.J. Jones, J. Rozière, Int. J. Hydrol. Energy 39 (2014) 6307–6316.
- [14] S. Siracusano, V. Baglio, N. Van Dijk, L. Merlo, A.S. Aricò, Appl. Energy 192 (2017) 477–489.
- [15] A.S. Gago, S.A. Ansar, B. Saruhan, U. Schulz, P. Lettenmeier, N.A. Cañas, P. Gazdzicki, T. Morawietz, R. Hiesgen, J. Arnold, K.A. Friedrich, J. Power Sour. 307 (2016) 815–825.
- [16] H.-Y. Jung, S.-Y. Huang, B.N. Popov, J. Power Sour. 195 (2010) 1950–1956.
- [17] H.-Y. Jung, S.-Y. Huang, P. Ganeshan, B.N. Popov, J. Power Sour. 194 (2009) 972–975.
- [18] V. Antonucci, A. Di Blasi, V. Baglio, R. Ornelas, F. Matteucci, J. Ledesma-Garcia, L.G. Arriaga, A.S. Aricò, Electrochim. Acta 53 (2008) 7350–7356.
- [19] V. Baglio, R. Ornelas, F. Matteucci, F. Martina, G. Ciccarella, I. Zama, L.G. Arriaga, V. Antonucci, A.S. Aricò, Fuel Cells 9 (2009) 247–252.
- [20] D. Aili, M.K. Hansen, C. Pan, Q. Li, E. Christensen, J.O. Jensen, N.J. Bjerrum, Int. J. Hydrol. Energy 36 (2011) 6985–6993.
- [21] A.V. Nikiforov, I.M. Petrushina, E. Christensen, A.L. Tomás-García, N.J. Bjerrum, Int. J. Hydrol. Energy 36 (2011) 111–119.
- [22] A.V. Nikiforov, A.L. Tomás García, I.M. Petrushina, E. Christensen, N.J. Bjerrum, Int. J. Hydrol. Energy 36 (2011) 5797–5805.
- [23] W. Xu, K. Scott, S. Basu, J. Power Sour. 196 (2011) 8918–8924.
- [24] M.K. Hansen, D. Aili, E. Christensen, C. Pan, S. Eriksen, J.O. Jensen, J.H. von Barner, Q. Li, N.J. Bjerrum, Int. J. Hydrol. Energy 37 (2012) 10992–11000.
- [25] P. Mazíř, J. Polonský, M. Paidar, K. Bouzek, Int. J. Hydrol. Energy 37 (2012) 12081–12088.
- [26] V. Natarajan, S. Basu, K. Scott, Int. J. Hydrol. Energy 38 (2013) 16623–16630.
- [27] H. Li, T. Fujigaya, H. Nakajima, A. Inada, K. Ito, J. Power Sour. 332 (2016) 16–23.
- [28] H. Li, A. Inada, T. Fujigaya, H. Nakajima, K. Sasaki, K. Ito, J. Power Sour. 318 (2016) 192–199.
- [29] J. Malíš, P. Mazúř, M. Paidar, T. Bystron, K. Bouzek, Int. J. Hydrol. Energy 41 (2016) 2177–2188.
- [30] A. Marshall, S. Sunde, M. Tsyplkin, R. Tunold, Int. J. Hydrol. Energy 32 (2007) 2320–2324.
- [31] A. Marshall, B. Borresen, G. Hagen, M. Tsyplkin, R. Tunold, Electrochim. Acta 51 (2006) 3161–3167.
- [32] C. Rozain, E. Mayousse, N. Guillet, P. Millet, Appl. Catal. B 182 (2016) 123–131.
- [33] B.-S. Lee, H.-Y. Park, I. Choi, M.K. Cho, H.-J. Kim, S.J. Yoo, D. Henkensmeier, J.Y. Kim, S.W. Nam, S. Park, K.-Y. Lee, J.H. Jang, J. Power Sour. 309 (2016) 127–134.
- [34] B.-S. Lee, S.H. Ahn, H.-Y. Park, I. Choi, S.J. Yoo, H.-J. Kim, D. Henkensmeier, J.Y. Kim, S. Park, S.W. Nam, K.-Y. Lee, J.H. Jang, Appl. Catal. B 179 (2015) 285–291.
- [35] H.S. Oh, H.N. Nong, T. Reier, A. Bergmann, M. Gliech, J. Ferreira de Araujo, E. Willinger, R. Schlogl, D. Teschner, P. Strasser, J. Am. Chem. Soc. 138 (2016) 12552–12563.
- [36] E. Slavcheva, G. Borisov, E. Lefterova, E. Petkucheva, I. Boshnakova, Int. J. Hydrol. Energy 40 (2015) 11356–11361.
- [37] S. Siracusano, V. Baglio, C. D'Urso, V. Antonucci, A.S. Aricò, Electrochim. Acta 54 (2009) 6292–6299.
- [38] J.M. Kahk, C.G. Poll, F.E. Oropeza, J.M. Ablett, D. Ceolin, J.P. Rueff, S. Agrestini, Y. Utsumi, K.D. Tsuei, Y.F. Liao, F. Borgatti, G. Panaccione, A. Regoutz, R.G. Egddell, B.J. Morgan, D.O. Scanlon, D.J. Payne, Phys. Rev. Lett. 112 (2014) 117601.
- [39] Y. Lu, T. Wang, Z. Cai, Y. Cao, H. Yang, Y.Y. Duan, Sens. Actuators B 137 (2009) 334–339.
- [40] M. Yagi, E. Tomita, T. Kuwabara, J. Electroanal. Chem. 579 (2005) 83–88.
- [41] M.A. Petit, V. Plachon, J. Electroanal. Chem. 444 (1998) 247–252.
- [42] J. Hämäläinen, T. Hatanpää, E. Puukilainen, T. Sajavaara, M. Ritala, M. Leskelä, J. Mater. Chem. 21 (2011) 16488.
- [43] K. Gobbel, T. Kuenzel, A. van Ooyen, W. Baumgartner, U. Schnakenberg, P. Braunig, Biomaterials 31 (2010) 1055–1067.
- [44] Zen Yoshimitsu, Akira Nakajima, Toshiya Watanabe, K. Hashimoto, Langmuir 18 (2002) 5818–5822.
- [45] J. Liu, A. Alfantazi, E. Asselin, Corrosion 71 (2015) 352–366.
- [46] J. Liu, A. Alfantazi, E. Asselin, J. Electrochem. Soc. 162 (2015) C189–C196.
- [47] D. Devilliers, M.T. Dinh, E. Mahé, D. Krulic, N. Larabi, N. Fatouros, J. New Mater. Electrochem. Syst. 9 (2006) 221–232.